Efficient energy based modeling and experimental validation of liquid filling in planar micro-fluidic components and networks

I. Treise, N. Fortner, B. Shapiro* and A. Hightower

This paper presents a model that describes how liquid flow fills micro-fluidic components and networks. As an alternative to computational fluid dynamic (CFD) simulations, we use a constrained energy minimization approach. This approach is based on two assumptions that hold in many micro-fluidic devices: (i) The length scales are small, and we consider slow filling rates, hence fluid momentum and viscous terms are small compared to surface tension forces, consequently the liquid/gas interfaces can be viewed as a succession of quasi-steady equilibrium configurations. (ii) Any equilibrium configuration corresponds to a surface tension energy minima which is constrained by the device shape and the volume of liquid in the device. The model is developed for planar micro-fluidic devices, is based on a fundamental physical principle, and shows accurate agreement with experimental data. It takes us only a few minutes to evaluate the model for a planar component of any shape using the Surface Evolver software, and this is significantly less then the computer run time required for CFD simulations. Moreover, once a library of component models has been created (which takes less than an hour of computer time) it then takes only seconds to simulate different network architectures with thousands of components. This fast 'reconfigure the network and simulate in seconds' capability is essential for the design of truly complex networks that will enable the next generation of passive, micro-fluidic, lab-on-a-chip systems.

1 Introduction

Soft lithography and polymer fabrication techniques[1–9] are well suited to the goal of creating low-cost, disposable, passive (no electrical power and no moving parts) micro-fluidic lab-on-a-chip systems. Passive systems typically rely upon the balance of surface tension and fluid pressure forces to perform their function. In particular, it is possible to exploit surface tension forces to create passive micro-fluidic valves and metering systems.[10–12] As a liquid fills any given component, the geometry of the component will cause the advancing liquid/gas interface to undergo a variety of shapes. Different shapes will create different pressures that will oppose or aid the liquid in filling that component. By intelligently designing the shape of a variety of components, it is possible to create sequenced valves: as the pressure is increased, component A will allow liquid to pass through before component B but only after component C. Such surface tension valves can then be used to make passive metering systems: an injected fluid will proceed along channel 1 until it encounters a strong surface tension valve at point 3, then point 2 (behind point 3) will break and the remaining liquid in channel 1 will be siphoned off to a waste chamber leaving behind a precisely metered volume in channel 1. Since it is possible to include passive (no electrical power) pressure actuators in micro-fluidic chips, for example by osmotic pressure,[13] by pressurized air reservoirs,[14] or by thumb actuated vials, the surface tension passive valves and metering systems enable a wide array of

behavior in a low-cost, disposable chip that does not require electrical power.

For real-world applications, the ultimate goal is to design and fabricate passive networks with many thousands of components to allow a tremendous amount of functionality in a single chip. It is possible to approach this chip design task in one of two ways: (i) single components can be designed and characterized based on experiments and then the networks can be designed 'by hand' or (ii) models can be created that describe the link between component geometry and filling behavior and then the networks can be designed using mathematical analysis and optimization tools. The first approach works well for small networks but it rapidly becomes impractical as the number of components increases: in our past research we have found that even a ten component network is beyond the limits of a 'by hand' design.[15] The second approach can, in principle, allow the design of networks with numerous components: in electrical engineering, the SPICE software package aids in the analysis and design of circuits with hundreds of thousands of components.[16] However, for this approach to work, there must exist computationally fast and accurate models of fluid filling in individual micro-fluidic components. This paper develops such models, validates them against experiments, and validates their use in the prediction of fluid filling in a small network. It is also demonstrates that the approach can simulate networks with thousands of components in seconds of computer run time. (The energy minimization approach also works for cases where the flow is being driven by electrical, as opposed to pressure, forces.[17,18] This scenario is

*benshap@eng.umd.edu

appropriate for chips with no moving parts but with electrical power.)

The paper is divided into three main sections: device fabrication and experimental methods, the energy based fluid filling modeling, and a comparison between theory and experiment.

Section 2 describes the fabrication technique: we use a plotter to cut patterns into sheets of vinyl and then we sandwich the vinyl sheets between Plexiglas and scotch tape layers to create planar devices. The approach is easy to use and inexpensive, and is similar to the one described in ref. 19. Section 2 also provides a characterization of the device roughness and geometry variations and it describes the experimental methods we use to fill the devices with liquid. The plotter fabrication technology has been chosen for two basic reasons. First, it provides a fast fabrication time (on the order of one hour), and this has allowed us to test the agreement between experiments and theory for a large variety of component shapes. Second, we intentionally chose a fabrication technique that creates components with a moderate degree of surface roughness and geometry variations (see Section 2.2). Since we have shown that our modeling approach works for such devices, it is likely that it will also work for devices with tighter engineering tolerances. We also note that there are a variety of other appropriate, low-cost fabrication techniques available, see for example ref. 1–9.

The modeling energy minimization framework is presented in Section 3. It relies on two central notions: first, the device length scales are sufficiently small and the fluid fills sufficiently slowly that fluid momentum and viscous effects are negligible; and second, the resulting quasi-steady equilibrium fluid states correspond to surface tension energy minima. Sections 3.1 and 3.2 describe the assumptions and the basic modeling approach. Section 3.3 transforms the energy minimization from a 3-dimensional problem to a 2-dimensional optimization appropriate for planar devices. Modeling results for single components are shown and discussed in Sections 3.4 and 3.5: the results are ordered from the simplest to the most complex component shapes. Each component model can be solved in minutes using the Surface Evolver program[20] and provides two key results: the succession of liquid/gas interfaces that will fill that component, and the (minimal, equilibrium) energy of each shape that is referenced to the corresponding volume of liquid in the component. From a network point of view, each component is completely characterized by the resulting 'energy *versus* volume' curve, so, once a library of component models has been created, it is possible to reconfigure and solve network models using these $E(V)$ curves in seconds of computer run time. In Section 3.6, we show an example where we predict the filling of a network with 10,000 components in 7 seconds of computer simulation time. Filling dynamics, the rate of filling of the network, is not included in the model: we simply find the liquid configuration for each liquid volume V, we do not provide equations for dV/dt.

Section 4 compares our theoretical modeling results with experimental data. We have fabricated a number of single component and small networks micro-fluidic devices to validate our modeling approach. Large networks are beyond the capability of our current fabrication techniques:

a comparison of theory and experiment for networks with thousands of components will be addressed in future research.

Our modeling approach allows the fast simulation of multi-component networks because it focuses on a specific physical scenario (quasi-steady network filling on the micro scale) and because we have found a way of phrasing that scenario in a mathematically tractable fashion (as a two-step 'component then network' optimization problem). Surveys of approaches for simulation of more general two-phase fluid flow settings can be found in ref. 21–28. The methods range from Volume-Of-Fluid (VOF) approaches, to explicit interface tracking schemes using marker particles and interpolations, to implicit Level-Set methods that represent the interfaces as the zero set of a higher dimensional function advected with the flow, and to particle model methods that represent the two fluids by a finite number of particles with interaction rules. Required simulation times vary, but typically, such methods solve a very large number of coupled nonlinear equations and require hours, or sometimes even days, of computer run time.

Model reduction is an alternate, and complementary, approach for creating fast models of two-phase flows. The idea here is to start with a first principles two-phase fluid flow simulation, and then to dramatically reduce the number of free variables in the simulation by projecting the governing equations onto a set of carefully chosen modes. If done successfully, this results in a dramatically faster model with only a small loss in simulation accuracy. There is a large body of research on model reduction techniques,[29–39] and there are many successful demonstrations of model reduction techniques applied to fluid dynamics problems, both for micro- and macro-scale scenarios.[40–43]

There also exist modeling results focused specifically on flow filling in micro-fluidic devices. Puntambekar *et al.*[12,14] present a finite element CFDRC (CFD research corporation, Huntsville, Alabama, USA) model of flow filling in passive valves. Tseng *et al.*[44] present CFD models for fluid filling of reservoirs which they compare with their experiments. Przekwas *et al.*[45] present a CFD computational methodology for describing flow in micro-fluidic devices with free surfaces. And Kim *et al.*[46] show experiments and CFD results using channel and cavity elements for micro-channel filling. They include the effects of surface tension, viscosity, and also fluid inertia terms that we do not consider in this paper.

2 Description of the planar micro-fluidic devices

This section describes how the micro fluidic devices are created (Section 2.1), provides the results of microscope and optical profile characterizations of the geometry variations and surface roughness of the devices (Section 2.2), and describes the experimental methods used to fill the devices with liquid and to measure the resulting liquid/gas interfaces (Section 2.3 and 2.4). The results of the filling experiments are compared with the theory of Section 3 in Section 4.

2.1. Fabrication of the planar micro-fluidic devices

The planar micro-fluidic devices are fabricated using three basic components: a vinyl layer with material removed to

create micro-channels, a Plexiglas backing with inlet and outlet holes for the fluid, and an adhesive tape covering layer. These components are assembled in a sandwich. The overall approach is similar to the one outlined in ref. 19.

The fabrication begins by creating the channel design for the middle layer of the sandwich that is a 70 μm thin vinyl film (Oracle Economy distributed by SignWarehouse). The vinyl has adhesive on one side and is lightly adhered to a silicone-coated paper from which it is easily removed. Once the micro-channel design is drawn in a Windows application called SignGo (by Wissen UK Inc.), it is transferred to a vinyl cutter (12″ Vinyl Express LYNX™ Desktop, distributed by SignWarehouse). The cutter has accurate control, which allows lines, circles, and arcs to be cut smoothly into the vinyl.

By controlling the cut speed, the blade cutting angle (choices are 30°, 45°, and 60°), and by adjusting the force on the blade, the cutter can cut materials with a maximum thickness of 0.03 inches (0.762 mm). Plotter motions are accurate within a few microns, but are limited to x and y *changes* of 30 μm by the resolution of the SignGo software. To guarantee a high quality cut, the blade has to be changed regularly to limit the effects of blade abrasion.

After finishing the cutting process, the interior area of the channels must be peeled off (Fig. 1a and b). Next, the vinyl must be attached with the adhesive side on a piece of Plexiglas (polymethylmethacrylate PMMA). The Plexiglas (2 mm thick) has the same size as the vinyl layer and contains pre-drilled holes (diameter ∼ 2 mm) for fluid injection and outlet. The application tape is used to transfer the channels to the Plexiglas without damage. This is done as follows: the application tape is attached to the vinyl, then the tape and the vinyl are gently pulled off from the vinyl base paper and attached to the Plexiglas (Fig. 1c–e). Once the vinyl is on the Plexiglas, the application tape is removed and an adhesive tape (Scotch Packaging) is used to seal the channels from the opposite side (Fig. 1f). When attaching the vinyl to the Plexiglas, step e in Fig. 1, embedded air bubbles between the layers must be removed with a squeegee.
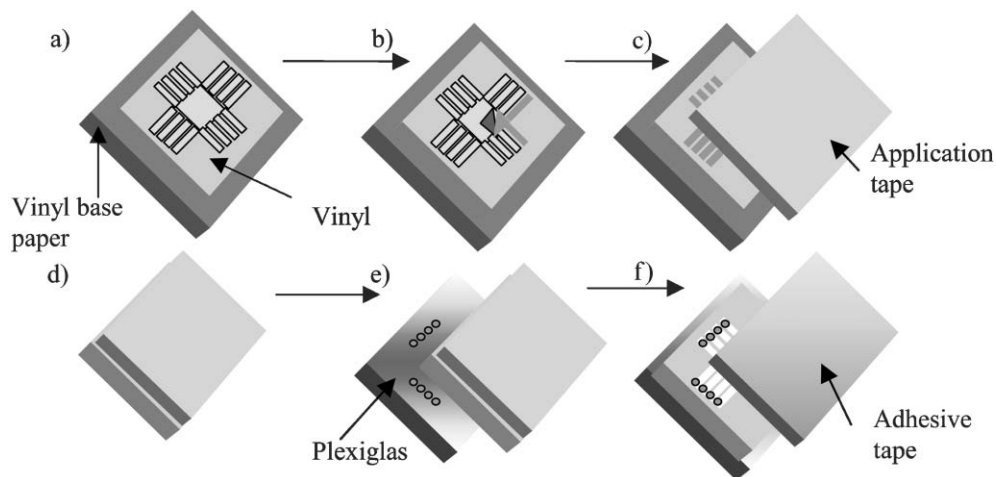
This technique of fabrication enables the production of low-cost micro-fluidic devices in less then two hours. It is possible to create straight channels with a minimum width of 30 μm (this dimension is a limitation of the resolution due to the SignGo software), and also channels with curves and sharp bends with radius of curvatures down to 60 μm. The sidewalls of the channels show a roughness of about 4 μm caused by the razor blade cutting action and blade tracking control inaccuracies. The channel depth depends on the thickness of the vinyl layer. Currently, the available thicknesses range between 50 and 70 μm.

2.2. Characterization of device geometry and surface roughness

The surface roughness of a sample channel was measured with a Veeco Wyko NT 3000 Optical Profiler and analyzed with Wyko Vision 32 Version 2.210 software. The average channel cross-sesction was measured to be 449 ± 8 μm by 69 ± 1 μm. The sidewall surface roughness was difficult to measure. Estimates were obtained from images taken with a Nikon Eclipse ME600 microscope. Features from three different regions and three different depths of focus (nine images total) were measured and averaged. Table 1 summarizes the measurement results.

2.3. Experimental methods for filling the micro-fluidic devices

The Plexiglas and vinyl materials are mildly hydrophilic, and so the channels/networks fill themselves under the influence of

Table 1 Summary of surface roughness measurements of a sample polymer microfluidic channel. Here: Ra = average roughness, Rq = root mean square roughness, Rz = average maximum height of profile, and Rt = maximum peak to peak height

	Ra/nm	Rq/nm	Rz/μm	Rt/μm
Substrate (floor)	73.21	163.64	4.27	5.000
Adhesive (ceiling)	207.44	291.24	7.8	13.15
Channel sidewalls	4200	5300	7	15

Fig. 1 Assembly of the device; (a) channel design is cut in vinyl; (b) vinyl is peeled off; (c)–(e) transfer of the channel to the Plexiglas by use of an application tape; (f) channel is sealed with an adhesive tape.

capillary forces. In order to fill the channels in this way, the water is injected into the holes of the Plexiglas which serve as fluid reservoirs. After the fluid comes in contact with the bottom layer of the device it slowly creeps along the walls of the channels towards the exit. Typically, we use red food color (Mc Cormick), whose main ingredients are water, propylene glycol and a red dye to visualize the liquid and to see the progressing liquid/gas fronts in the devices. A camera records the motion of the colored fluid for subsequent analysis and interpretation.

Before first using the device, it is important to remove all dust particles in the channels which deposit during fabrication. The cleaning proceeds by flushing the channels with ethanol using a vacuum pump and waiting until the channels are dry. Each device can be used multiple times, but it is necessary to clean the device with ethanol after each use.

2.4. Experimental methods for measuring liquid/gas interfaces in the devices

Liquid/gas interfaces are measured using a CCD Camera (Digital Camera Vision Components Ettlingen, Germany) with an integrated DSP (Digital Signal Processor). The DSP is dedicated to Image Processing and to transferring the pixilated image data from the camera to the host computer. The camera is mounted on a Bausch & Lomb microscope with a magnification of $\times 60$ (objectives: 3X, 20X). Using a Video Converter (StarTech.com) and an external USB TV connection (AverMedia) the experiment images can be recorded as AVI files. These AVI files are imported into Matlab and are processed using the image processing toolbox to find the location and shape of the liquid/gas interfaces.

To find the (effective planar) surface tension coefficient for the devices, when filled with water or with any other liquid, we compare the liquid/gas filling fronts in a simple channel experiment with the minimum energy model of Section 3. This technique selects the surface tension coefficient of eqn. (3) that bests fits the experimental data. This process is carried out one time for each type of fluid (the same solid materials are used for all our devices). This comparison method is equivalent to directly measuring the contact angle found in the planar devices but it is more accurate and it directly provides the single unknown material dependent coefficient γ that is necessary for our modeling.

As a way to check our values for the planar surface tension coefficient we also measured the contact angles of the liquid (deionized water and methanol) with respect to the floor, ceiling, and wall materials of our devices. The angles were measured using the sessile drop method in air using a goniometer coupled with an American Optical AO569 Stereo Microscope and a digital camera Oympus C-4000 digital camera. Two droplets were tested and averaged for each surface. The wall contact angle measurements are suspect because we had to stack up 60 layers of vinyl sheets in order to get a sufficiently large area to perform the tests, and it is quite likely that the interface created in this way is not a true reflection of the channel wall surface tension characteristics found in our devices. Nevertheless, the value we get for the planar surface tension coefficient γ of eqn. (3) is consistent with the experimental values in Section 4.

3. The energy based component filling modeling framework

Our modeling goal is to find the shape of the liquid/gas interfaces as the liquid fills planar, single or multiple, components with arbitrary geometries. Further, we desire a model that is sufficiently accurate to enable engineering analysis and design but that evaluates adequately fast to enable the simulation of thousands of coupled components—our end goal is to simulate, analyze, and design the filling of complex micro-fluidic networks.

The energy minimization modeling approach that we use is based on two observations. First, the network is filled slowly by capillary forces hence we treat the propagating liquid/gas interfaces as a succession of quasi-steady equilibrium configurations. The succession of equilibrium states is parameterized by the amount of liquid in the device: each equilibrium state corresponds to a specific volume of liquid. Second, stable (or unstable) equilibrium shapes correspond to minima (or maxima/saddles) of the surface tension potential energy.[47–49] This means that we can phrase the equilibrium shape problem as an optimization problem with filled volume and device geometry constraints. We are able to solve this optimization task quickly and accurately.

3.1. The filling rate and the validity of the quasi-steady assumption

The validity of our quasi-steady assumptions depends on size of the micro-fluidic network and the rate of filling. To estimate the permissible rate of filling of the network before the quasi-steady model fails, we proceed as follows. The analysis below holds either for self-filling by capillary forces or for forced filling via a syringe or a pump. We consider a network with n channels of average length l and radius r. For such a network, the viscous forces, and hence the order of magnitude of any applied pressure/momentum forces that are used to drive the flow at a prescribed volume flow rate, scale as $F_{\text{visc}} \sim (\mu U/r)A_{\text{visc}} \sim (\mu U/r)(2\pi rnl) \sim \pi\mu nlU$ where μ is the viscosity of the fluid, U is the velocity of the fluid, and $A_{\text{visc}} = 2\pi rnl$ is the contact area over which the viscous stresses act. The quasi-steady theory will fail when the momentum forces first approach the size of the surface tension forces inside each channel. The surface tension forces scale as $F_{\text{ST}} \sim A\,\sigma/R \sim \pi\sigma r$ where $A = \pi r^2$ is the cross section area and $R \sim r$ is the radius of curvature of the interface. The momentum forces are comparable to the viscous forces. Hence the quasi-steady theory is valid when $\frac{F_{\text{visc}}}{F_{\text{ST}}} = \frac{nl}{r}\frac{\mu U}{\sigma} = \frac{nl}{r}Ca \ll 1$ where $Ca = \mu U/\sigma$ is the capillary number, or equivalently, when $U \ll \frac{r}{nl}\frac{\sigma}{\mu}$. Water has a viscosity of $\mu = 10^{-3}$ kg ms^{-1} and the water/air surface tension coefficient is $\sigma = 0.72 \times 10^{-3}$ kg s^{-2},[47] so for the filling of micro-fluidic networks with water displacing air we require $U \ll (r/nl)\,0.72$ m s^{-1} for the quasi-steady theory to hold. For the networks considered in this paper, we have channels with

approximate length $l \sim 1$ cm and radius $r \sim 100$ μm, and we treat up to ten channels at once $n \leqslant 10$. Thus we need $U \ll 0.72$ mm s^{-1} which means it would take us about one or two minutes to fill a network with channels of length 1 cm (120 s is much greater than the 1 cm/0.072 cm s^{-1} = 13.8 s). In the experiments, we fill the networks in about five to seven minutes to guarantee that the quasi-steady assumption remains valid. For future, faster network filling applications we are extending our methods to include computationally cheap (reduced order) models of viscous effects. This will enable us to move beyond the quasi-steady assumption used in this paper.

We also note that there are friction forces due to the moving contact line that we do not consider here. It is expected that such forces will become important near the walls, floor, and ceiling, and they will have a substantial overall effect on the liquid shape only for devices with very small filling lengths. For a description of moving contact line friction forces see, for example ref. 50–52.

3.2. The basic approach: minimization of the surface tension potential energy under device geometry and enclosed liquid volume constraints

At every instant in time the liquid/gas interface equilibrium configurations are viewed as the minima of the surface tension potential energy. Viewing spherical liquid droplet shapes and interface contact angles as minimum energy surfaces is customary and it is consistent with the methods described in ref. 20,47–49. Our approach of viewing any equilibrium liquid/gas interface as an energy minimum is a natural extension, and it is a subset of the far more general concept that all equilibrium configurations, for almost any kind of system, correspond to energy minima.[53] As noted by Feynman,[53] net forces are the derivatives of the energy with respect to shape parameters, so the forces balance if and only if the system potential energy is at a stationary point.

Our main contribution is to effectively apply the above energy minimization idea in complex (but planar) devices and networks. We do this by finding the interface shape that minimizes the surface tension energy cost subject to constraints imposed by the device geometry and by the amount of fluid

that has been injected or sucked into the device. For example, if we have a twisted T geometry which contains thirty microliters of liquid, we find the liquid/gas interface shape by solving an optimization problem that minimizes the surface tension energy subject to the constraints that the interface be confined inside the twisted T and encloses exactly thirty microliters of liquid. At the next instant in time we repeat the process for thirty one microliters of fluid. A schematic of this approach is shown in Fig. 2.

To do the above we must define the potential energy of the micro-fluidic systems as a function of interface shapes. The potential energy we consider consists of surface tension effects only. Gravity effects are ignored due to the small size of the devices. As in ref. 47,48, we model the energy per unit area of each liquid/gas, liquid/solid, and solid/gas interface *via* a material dependent surface tension coefficient. This gives the potential energy as

$$E = \int_{L \cap G} \sigma_{LG} dA_{LG} + \int_{L \cap S} \sigma_{LS} dA_{LS} + \int_{S \cap G} \sigma_{SG} dA_{SG} \quad (1)$$

where S, L, and G are the domains in three-dimensional space occupied by solid, liquid, and gas phase respectively, ∪ denotes their intersections (so L∪S is the two-dimensional liquid/solid interface), and σ_{AB} denotes the associated interfacial potential energy per unit area. The surface tension energy formulation of eqn. (1) is acceptable so long as the device length scale is large compared to the interface thickness. This is certainly the case in our networks with micrometer sized components.

3.3. Rephrasing the energy optimization problem in two spatial dimensions

For any thin planar device, such as the one shown in Fig. 3, it is safe to assume that the top to bottom liquid/gas interface profile is constant.[15] With this assumption it is possible to convert the liquid front filling problem from three spatial dimensions down to two. Let p be the arc length of the vertical interface profile. Then the liquid/gas interface area is given by $A_{LG} = |L \cup G| = pS$ where |·| denotes the area of an interface and where S is the average arc length of the interface in the
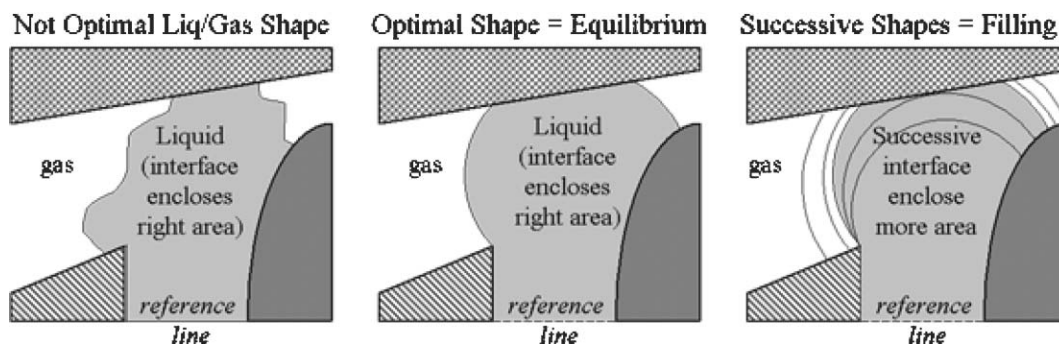

Fig. 2 Two-dimensional schematic of a sample planar solid geometry being filled by a liquid under surface tension: the different shadings of the three material blocks denote different surface tension properties. To find the equilibrium liquid/gas interface, we first consider all liquid/gas shapes that respect the shape of the device and that enclose the right amount of liquid (left); then we pick the equilibrium shape that minimizes the surface tension energy of eqn. (1) (middle); and finally we find such optimal shapes for a succession of liquid volumes to arrive at a component filling theory (right).
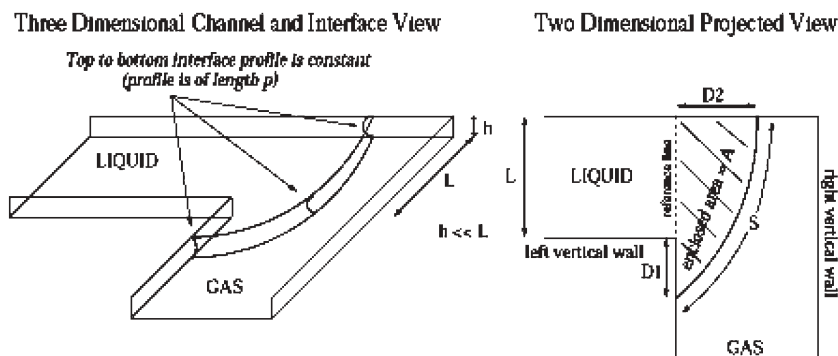
Fig. 3 An L-corner planar geometry. Due to the small vertical height of the device, a liquid/gas interface moving through this geometry will have a constant vertical interface shape: the interface shape will vary in the horizontal plane only.

horizontal plane (see, for example, Fig. 3). Here S varies as the liquid fills the component but p remains constant. Since the liquid/air surface tension coefficient is assumed constant, this reduced the first term in the potential energy of eqn. (1) to $\int_{L \cap G} \sigma_{LG} dA_{LG} = \sigma_{LG} A_{LG} = \sigma_{LG} pS$. Likewise it is possible to rewrite the liquid/solid and solid/gas potential energy terms solely in terms of horizontal dimensions. For example, in the L-corner, the wetted vertical liquid/wall surface areas are given by hD_1 and hD_2 where D_1 and D_2 are as shown in Fig. 3 and h is the vertical distance between the floor and the ceiling. The gas/wall surface areas are simply the total available wall areas minus the wetted liquid/wall areas. Finally, the floor–ceiling/liquid and floor–ceiling/gas contact areas are irrelevant to the shape energy minimization and they can be dropped from the energy cost. This is because, at any moment in time, the volume of liquid contained inside the device is treated as a constant and is given by $V = hA_{LS:FS}$, where $A_{LS:FC}$ is the contact area of the liquid with the floor and the ceiling. Since this floor/liquid plus ceiling/liquid contact area only depends on the amount of liquid currently contained inside the device, it is independent of the horizontal shape of the liquid/gas interface, and it can be dropped from the energy optimization cost.

The surface tension energy of eqn. (1) can now be rewritten in two spatial dimensions as

$$E_{2D} = S + \gamma_1 D_1 + \ldots + \gamma_k D_k \qquad (2)$$

$$(= S + \gamma D \text{ if all walls are of the same material})$$

where S is the mean horizontal arc length of the liquid/gas interface, and $D_1, D_2, \ldots, D_k$ are the wetted lengths of walls $1, 2, \ldots, k$ respectively. (For the planar L-corner, D_1 and D_2 are as shown in Fig. 3.) The parameters $\gamma_1, \gamma_2, \ldots \gamma_k$ are non-dimensional, material dependent, ratios of surface tension and geometry parameters. Specifically, for the jth wall:

$$\gamma_j = h(\sigma_{LS:Wj} - \sigma_{GS:Wj})/p\sigma_{LG} \qquad (3)$$

In our devices all walls are made out of a single type of material hence $\gamma_1 = \gamma_2 = \ldots = \gamma_k = \gamma$. We identify the single missing coefficient γ by finding the value γ that provides the best agreement between a straight channel experiment and a

straight channel energy model. The parameter γ is related to the observed contact angle in the horizontal plane by the analog of the Young equation $\gamma = -\cos\theta_{2D}$.[47] Thus eqn. (3) gives the contact angle in the horizontal plane as a function of the surface tension coefficients of the Plexiglas, vinyl, and the adhesive tape materials. In our devices, θ_{2D} varies between $105°$ and $112°$ degrees depending on the polymer manufacturer, handling, and experimental conditions that affect material and surface properties, surface roughness, temperature, and humidity.

3.4. Filling of a planar L-corner

Except for a straight channel where the filling is trivial to predict, the planar L-corner is the simplest possible geometry that can be considered. Detailed results for this case have been presented in our conference paper.[15] Below we briefly summarize the key results.

A cut away view of the planar L-corner geometry is shown in Fig. 3. As a special case of eqn. (2), the surface tension energy is given by $E_{2D} = S + \gamma_1 D_1 + \gamma_2 D_2$. We must minimize this energy subject to the liquid volume and device geometry constraints. The minimization is done in two parts. First, for any D_1 and D_2 we minimize the shape of a liquid/gas interface pinned at the D_1 and D_2 lengths. By the calculus of variations[54] we know that a circular arc is the required optimal shape because it minimizes arc length subject to an enclosed area constraint. The radius of this arc is uniquely determined by D_1, D_2, and by the amount of liquid that has been injected or sucked into the device at any time. Second, we find the optimal D_1 and D_2 lengths. In ref. 15 we parameterize D_1 and D_2 by the length $2l$ and orientation angle θ of the line segment between the arc starting and ending point since this provides a smoother parameterization of the energy cost then the D_1 and D_2 parameterization.

The L-corner surface tension energy $E_{2D} = S + \gamma_1 D_1 + \gamma_2 D_2$ is now a function of l and θ only. However, not all (l, θ) pairs are permitted: some pairs violate the geometry of the device (the arc intersects the walls at multiple points or fails to span the channel), and some pairs violate enclosed area requirements (for these (l, θ) pairs the arc radius cannot be chosen in a way that respects the devices geometry and encloses the correct amount of liquid). The geometric constraints on l and θ are

derived analytically in ref. 15. The resulting (l^*, θ^*) energy minimum corresponds to the equilibrium shape of the liquid/gas interface at a prescribed liquid volume. Using a gradient descent algorithm it takes about 2 seconds to find any such equilibrium front using Matlab on a desktop personal computer. By finding a succession of optimal (l^*, θ^*) pairs for increasing liquid volumes, we arrive at an L-corner filling theory. As shown in ref. 15 the agreement between theory and experiment for the L-corner is excellent.

It is important to compare our approach above with the two standard approaches of computational fluid dynamic (CFD) and stand alone contact angle methods. CFD approaches require a discretization of the (two-phase) Navier Stokes or Stokes fluid equation along with the tracking and computation of forces on a moving liquid/gas boundary. This is computationally expensive. A coarse 2-dimensional CFD simulation for a planar component might have 100 by 100 grid points with 3 variables (u, v, P) per node. That is a total of 30,000 equations that must be solved simultaneously for each time step. To better resolve the liquid/gas curvature, a mesh of a 1000 by a 1000 grid points may be needed: this yields 3 million equations. For this reason, Stokes flow two-phase simulations carried out in our laboratory for the L-corner geometry take two hours of computer run time per component. Simulation times quoted in the literature vary from hours to days. By comparison, the planar energy minimization proceeds by optimizing a surface (a curve) that is adequately defined by 2 variables for the L-corner and by 20 to 40 points for other component shape. Thus we iterate on less then 40 equations to find the interface at each time. Our energy minimization approach therefore takes seconds for the L-corner, minutes for more complex component shapes, and by using a two-stage approach, allows the simulation of networks in seconds.

Contact angle approaches specify the angle between the liquid/gas interface and the solid surface. If used on their own independently of CFD computations, then they are computationally trivial to implement but it is not clear how to use them to find liquid/gas filling fronts in non-trivial device geometries. This is true for a number of reasons that we list from the least to the most serious. First, one requires an equation to translate the three-dimensional contact angles (of water in air on vinyl, on Plexiglas, and on scotch tape) into one planar two-dimensional contact angle (see the discussion preceding eqn. (3)). This issue is minor: it is possible to circumvent it by simply measuring the contact angle in the planar geometries. Second, the contact angle condition is undefined or cannot be true at corners, at lines of symmetry, and at points where the liquid/gas front first impinges on a new solid surface. For example, in the T component geometry of Fig. 4, when the filling front first touches the opposite wall the contact angle is clearly 180° and not the 108° angle that would be prescribed elsewhere.

Third, and most serious of all, when using only a contact angle approach it is not known *where* to apply the contact angle conditions. For simple geometries such as straight channels, L-corners, and T shapes it is possible to finesse this issue by solving for the location of the liquid/gas/solid triple points by a combination of intuition and geometric inversion: for the L-corner one could argue, correctly, that the front first progresses as in a channel and that the triple points are symmetric across the channel, until the interface arrives at the corner, then the interface turns the corner (so the outside triple point sweeps around), and this continues until the inside contact angle matches the contact angle of the new inside wall, at which point the interface leaves the corner and proceeds down the new channel. For each of the three cases above one can find the location of the triple points so that the interface encloses the right amount of liquid volume. However, this requires that a human user examine the model for each component individually and it is not possible to extend this argument to more complex geometries such as the ones shown in Fig. 10 and Fig. 11 later. Our approach finds the location of the triple points as a part of the constrained optimization.

3.5. Filling of a single planar component of arbitrary shape

In this section we extend the L-corner results of the previous section to the filling of planar components of arbitrary shape. The basic approach is still the same: we seek minimum energy surfaces in two spatial dimensions that respect the device geometry and that enclose the right amount of liquid at any given moment. The main difficulty in transitioning from the L-corner to more complex shapes is the generalization of the (l, θ) constraint curves that delineate the allowable shape parameters. These constraints are derived by hand in ref. 15 and the analytic computations are lengthy and tedious even for the simple L-corner. They cannot be carried out for more complex shapes. We have chosen to circumvent this difficulty by using the Surface Evolver[20] software developed by Ken
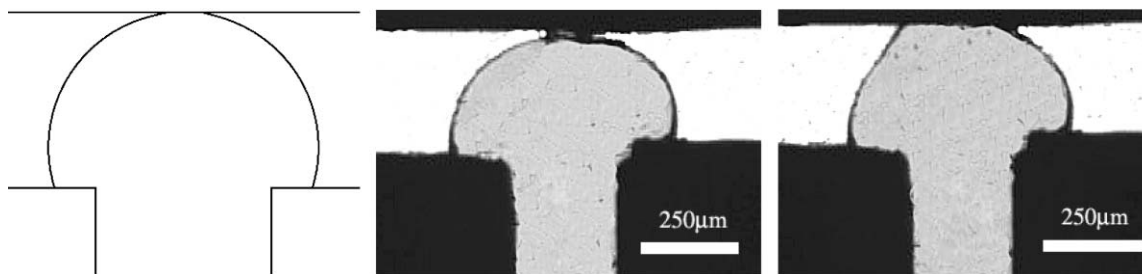

Fig. 4 The T geometry is a simple example of how the contact angle condition can fail at points of symmetry. In the above (a simulation based on the methods of Section 4 and two snapshots of an experiment) it is clear that a $\theta_{2D} = 108°$ contact angle condition fails when the liquid/gas interface first touches the top wall.

Brakke. This software finds minimal energy surfaces in two and three spatial dimensions subject to various costs and constraints. Surface Evolver defines surface as a union of triangles in three spatial dimensions or as a collection of line segments in two dimensions, it then evolves the surface in the direction of decreasing cost by using a (constrained) gradient descent algorithm.

We have successfully used Surface Evolver to predict liquid/gas filling fronts in our micro-fluidic components. The energy to be minimized is given by eqn. (2) where γ is the material dependent surface tension coefficient defined in eqn. (3) . For any component, we start the Surface Evolver optimization at an arbitrary interface shape defined by just three vertices. The first and last vertices are restricted to be at the component walls that act as geometric constraints. Surface Evolver then refines the shape of the interface by successively adding and moving the vertices to minimize the energy cost while enforcing both the geometry and imposed liquid volume constraints. Once convergence is achieved we increase the liquid volume and, using the previous solution as the new initial interface, we find a new optimal solution. This provides a succession of optimal liquid/gas interfaces that fill the component. Each simulation takes about 2–3 min to find the succession of fronts through simple geometries, more complex geometries require 6–8 min. Surface Evolver cannot guarantee that global energy minima have been found. However, for the component shapes used here, all the energy minima are physically meaningful and, to the best of our knowledge, correspond to global energy minima. Below we show results for a variety of planar components.

The top part of Fig. 5 shows a top view of a sample circular chamber component. Calculated liquid/gas interfaces are shown as thin numbered curves: we have only shown a small selection of the curves to illustrate how the solution changes when passing different geometrical features. The bottom panel of Fig. 5 shows the energy of the interfaces for a hydrophobic and hydrophilic circular chamber as a function of the amount of liquid volume in the component.

Fig. 6 and Fig. 7 show the simulated filling of a planar cross channel and an asymmetric branch channel. In each case, a simulation is done for both a hydrophobic and a hydrophilic case. As in the L-corner, it follows from the planar nature of the components, the simple choice of the surface tension cost in eqn. (2) , and the calculus of variations,[54] that all interface segments are circular arcs: only their number, radius, and locations vary as the component fills. Different components can show very interesting behavior: for instance, the branch component shows a retreat of a liquid/gas interface in one channel to preferentially fill another channel once the interface passes the channel branch point. We have also done simulations for a variety of other component shapes which are not included here due to space limitations.
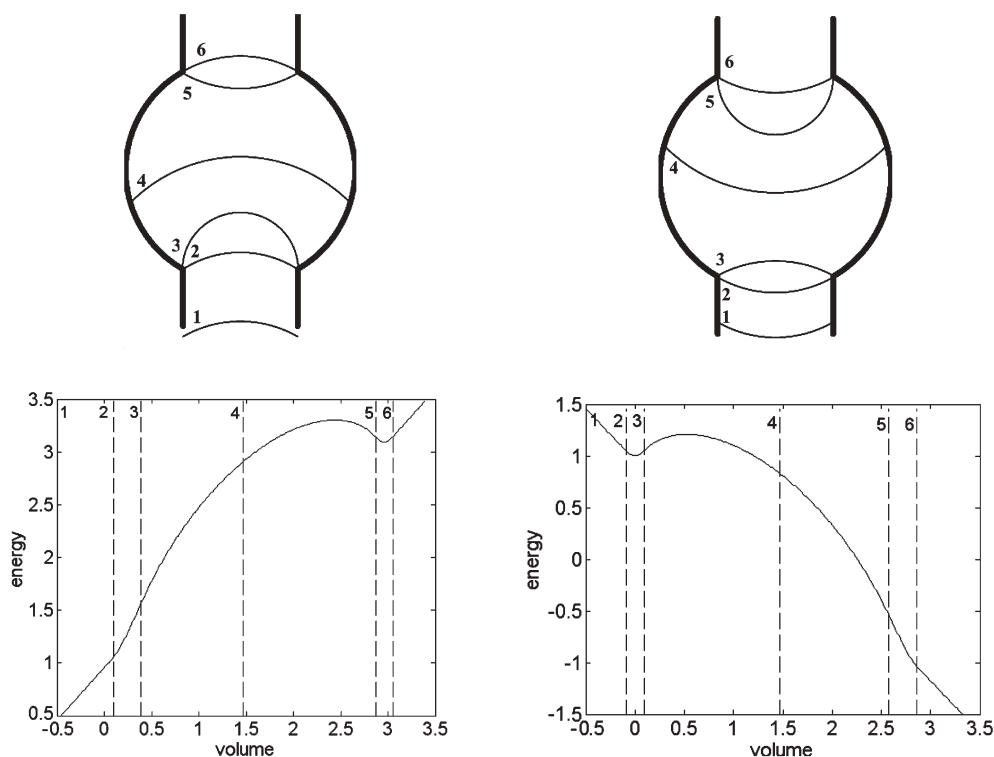

Fig. 5 Simulated filling of a planar circular chamber. Bold lines in the top panels show the component geometry. Top panels: The thin numbered curves show the progression of filling fronts for a hydrophobic material ($\theta_{2D} = 120°$; $\gamma = 0.5$) on the left and a hydrophilic chamber ($\theta_{2D} = 60°$; $\gamma = -0.5$) on the right. Bottom panels: The graphs show the minimal, equilibrium surface tension energy of the interfaces as they progress through the component. The volume was increased in increments of $\Delta V = 0.01$ since increments smaller then this did not substantially improve the simulation accuracy. The component on the left is hydrophobic so it takes energy to fill this device. The component on the right is hydrophilic and so energy must be expended to prevent it from filling.
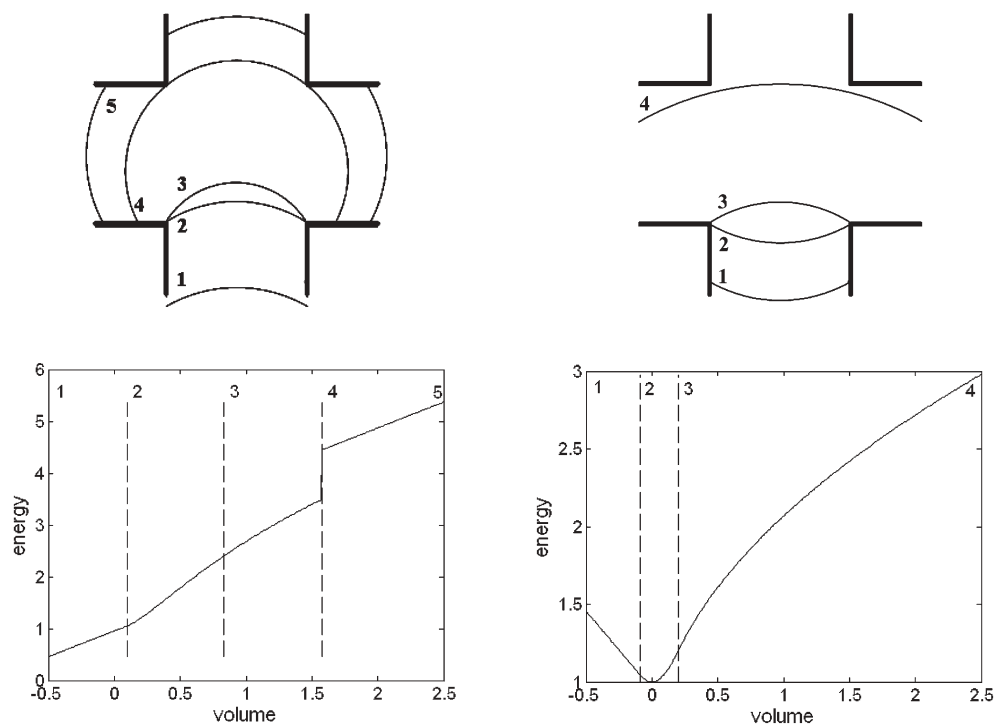
Fig. 6 Simulated filling of a cross channel component. The presentation format is the same as in Fig. 5. Left: hydrophobic behaviour: $\theta_{2D} = 120°$, $\gamma = 0.5$. Right: hydrophilic behaviour: $\theta_{2D} = 60°$; $\gamma = -0.5$. The liquid/gas interface splits from one circular arc (4) to three circular arcs (5) when the interface passes the corner points of the cross channel.
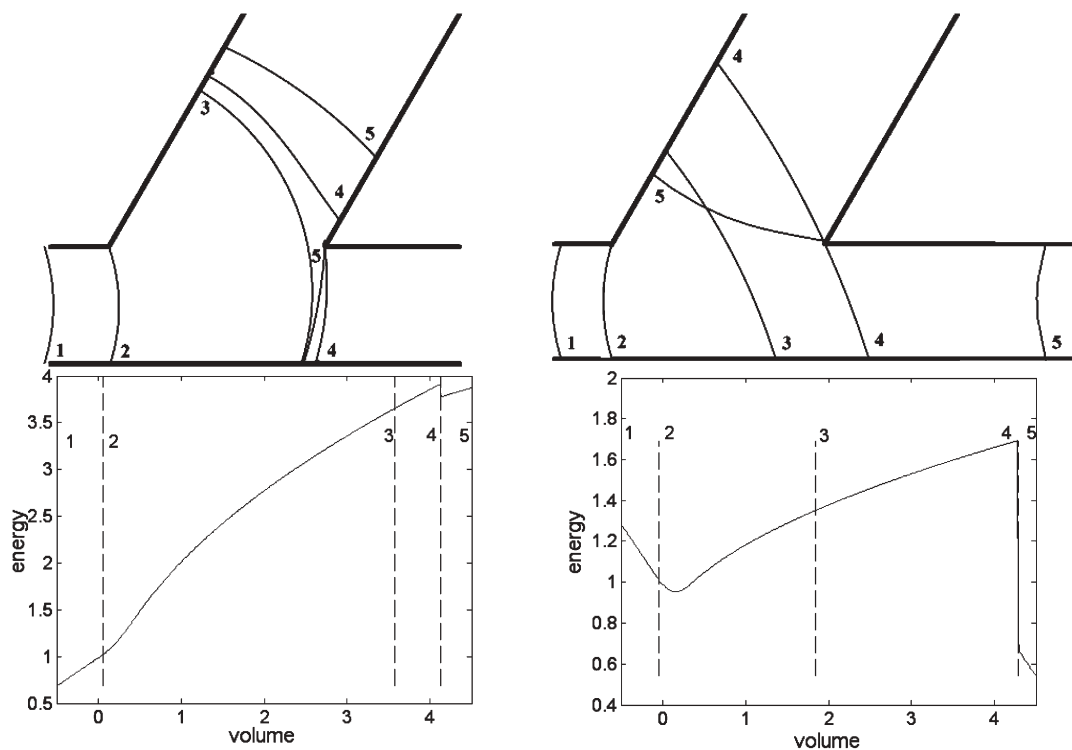

Fig. 7 Simulated filling of a branch component. The presentation format is the same as in Fig. 5. Left: hydrophobic behaviour: $\theta_{2D} = 107°$, $\gamma = 0.3$. Right: hydrophilic behaviour: $\theta_{2D} = 72°$; $\gamma = -0.3$. This component displays some interesting behaviour. For the hydrophobic (left) case: the interface prefers the wider channel, (interface 5 is ahead of interface 4 in the top channel) and it is withdrawn from thinner channel (interface 5 is actually behind 4 in the narrow bottom channel). For the hydrophilic case (right) the reverse happens: the interface is sucked into the narrow channel (5 is ahead of 4) and is sharply withdrawn from the wide channel (interface 5 has withdrawn all the way back to the mouth of the wide channel).

3.6 Filling of a hub network of planar components of arbitrary shape

We now turn to modeling fluid filling in a network of components. There are two possible ways to do this. The first option is to perform a Surface Evolver simulation with geometry constraints for the entire network: in this option we simply replace the geometry of Fig. 5–7 with the geometry of the entire network. This option is still less computationally intensive then a CFD 2-phase simulation, but it is still fairly expensive: a network with a hundred components would take about 10 hours. Below, we discuss an alternate two-stage approach that, once a library of component models has been built up, can simulate networks with thousands of components in seconds.

To simulate a network we must minimize the surface tension energy of numerous interfaces across multiple components. We already know how to find the minimal surface tension energy of any single component using the methods of Section 3.5. The bottom panels of Fig. 5–7 show this equilibrium energy as a function of the liquid volume in each component. From a network point of view, these energy *versus* liquid volume $E_j(V_j)$ curves completely characterize the behavior of each component. The total energy of a network with n components is now given by the sum of individual component energy *versus* volume functions

$$E = E_1(V_1) + E_2(V_2) + \ldots + E_n(V_n). \qquad (4)$$

For example, we may consider a network made out of four types of components (circular chambers, L-corners, cross channels, and branch splitters) in which case each $E_j(V_j)$ function above would be one of four curves, two of which are shown in Fig. 5 and Fig. 7. If the network included other types of components we would pre-compute their energy *versus* volume curves. Further, we know that the total network volume is given by

$$V_1 + V_2 + \ldots V_n = V. \qquad (5)$$

As the network fills, this total volume V goes from zero to the maximum fluid volume that can be contained in the network. The optimization task is to find the amount of fluid in the components $V_1, V_2, \ldots, V_n$ that minimizes the total surface tension energy of the network as the total fluid goes from zero to its maximum value. Per the estimates in Section 3.1, it is valid to treat the entire network as if it were going through a succession of equilibrium states so long as the self or imposed filling rate is sufficiently slow. To find the equilibrium component filling volumes V_j's as a function of the total volume V we must solve the following optimization:

$$\min \ E = \sum_{j=1}^{n} E_j(V_j) \ \text{ subject to } \ \sum_{j=1}^{n} V_j = V. \qquad (6)$$

This is a standard nonlinear, multi-variable, scalar cost, single constraint optimization.[55] Here we have assumed that all the components are connected to one central reservoir or injection point. Networks with multiple hubs would require multiple, interlinked sub-network component volume constraints. This would increase the number of constraints and would increase the simulation time slightly.

In summary, the network model proceeds in two parts. First, we generate a set of component simulations as in Section 3.5 using Surface Evolver. Since each component takes about 2 to 8 min to simulate, a network with thirty different types of components would require a total computer run time of between 1 and 4 hours. Second, once we have the $E_j(V_j)$ curves for all the components in the network, we solve the optimization stated in eqn. (6) using a constrained gradient descent algorithm. This takes seconds of computer run time using Matlab on a personal computer. The architecture of the network can now be changed and the behavior of the new network can be ascertained in seconds. Fig. 8 shows a simulation of a hub network with 10,000 components: each $E_j(V_j)$ curve of all the 10,000 components was randomly generated. The second part of the optimization, the part where we solve the optimization problem of eqn. (6), took 7 seconds of computer run time on a personal computer. A 10,000 component network is beyond our fabrication capabilities outlined in Section 2.1 but we compare the theory above to experimental filling of a small, four component, network in Section 4.
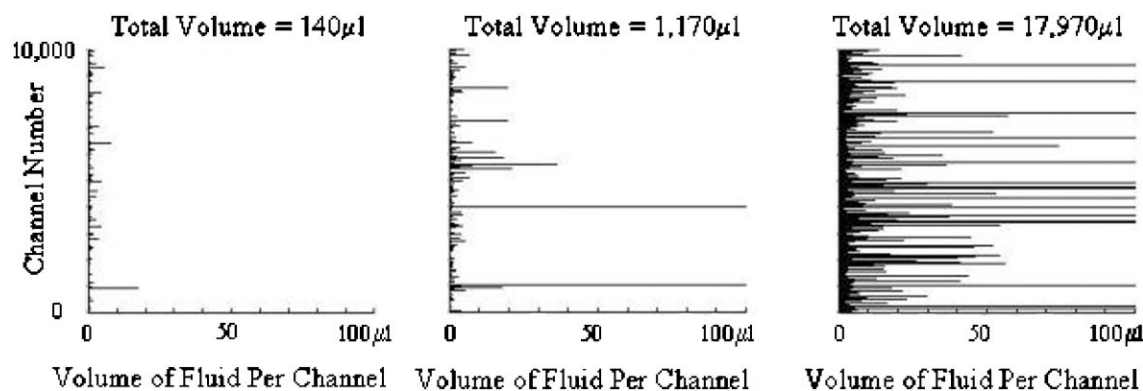

Fig. 8 Quasi-steady component filling for a network with 10,000 components. Each channel is described by a randomly generated $E_j(V_j)$ curve (see bottom panels of Fig. 5–7). The graph shows the fluid per channel for three amounts of injected total fluid V. Total computation time was 7 seconds on a personal computer.

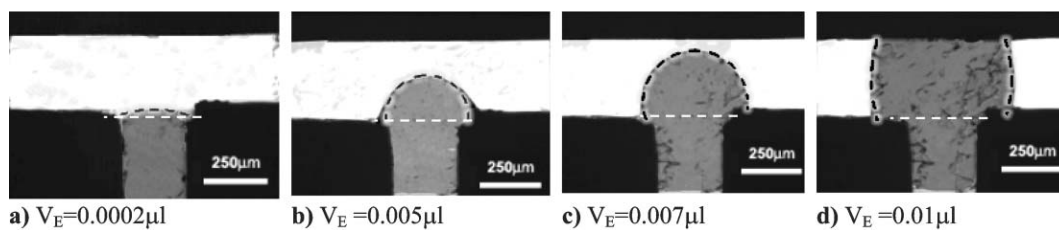**a)** V_E=0.0002µl   **b)** V_E=0.005µl   **c)** V_E=0.007µl   **d)** V_E=0.01µl

Fig. 9 Comparison of the theory (dashed line) and experiment (boundary between gray and white) for a T component. The energy filling Surface Evolver model of Section 3.5 is compared with a 250 µm wide, 70 µm deep T-junction channel fabricated using the techniques of Section 2.1. The model uses a planar surface tension contact angle of $\theta_{2D} = 94°$, or equivalently a non-dimensional surface tension coefficient of $\gamma = 0.07$ as written in eqn. (3). V_E is the volume of liquid inside the component at each time.

4. Model validation: theory *versus* experiments

In this section, we compare experimental results attained using the methods of Section 2 with the modeling approach described in Section 3. Besides the geometry of the component or network, the model requires two inputs, which are: the volume of liquid in the component or network, and the surface tension parameter γ of eqn. (3) or equivalently the planar contact angle θ_{2D} ($\gamma = -\cos\theta_{2D}$). The volume of liquid inside the component is known experimentally: we measure the filled area using image processing techniques and then we multiply this area by the depth of the device to find the contained liquid volume. The γ parameter of eqn. (3) depends on the height of the planar device and the type of solid and liquid materials being used. It is determined one time beforehand by comparing the theoretical prediction for the filling of a straight channel with an experiment.

Fig. 9 shows a comparison of theory and experiment for a T junction component. The visible discrepancy between the theory and the experiment is due to the imperfect shape of the 90° corners that are caused by the vinyl cutting inaccuracies. Fig. 10 shows the match between theory and experiment for a component of arbitrary shape.

In Section 3.6 we describe how to efficiently model the filling of networks. Fig. 11 shows a comparison of this two-step model *versus* a front filling experiment for a network with four components. There is accurate agreement between the model and the experiment.

5. Conclusion

The design and optimization of complex, passive, lab-on-a-chip devices requires modeling tools that can simulate complex networks with numerous components: it is not possible to
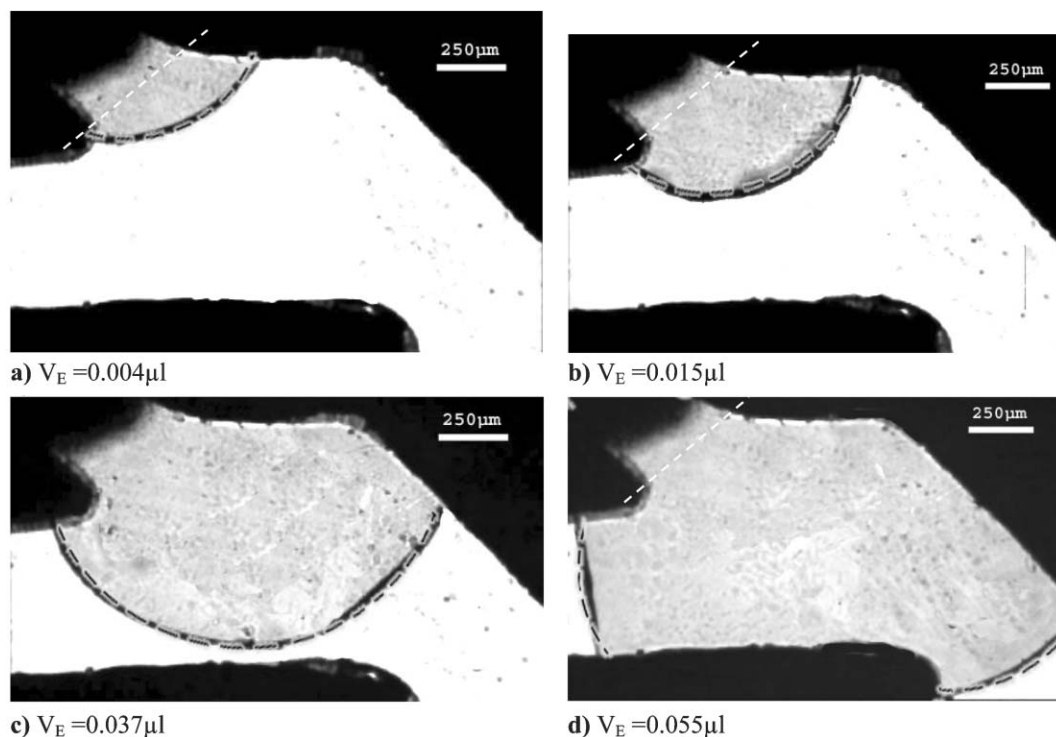

a) V_E=0.004µl

b) V_E=0.015µl

c) V_E=0.037µl

d) V_E=0.055µl

Fig. 10 Comparison of the theory (dashed line) and experiment for a component of arbitrary shape. The model parameter is $\theta_{2D} = 114°$ or equivalently $\gamma = 0.4$.
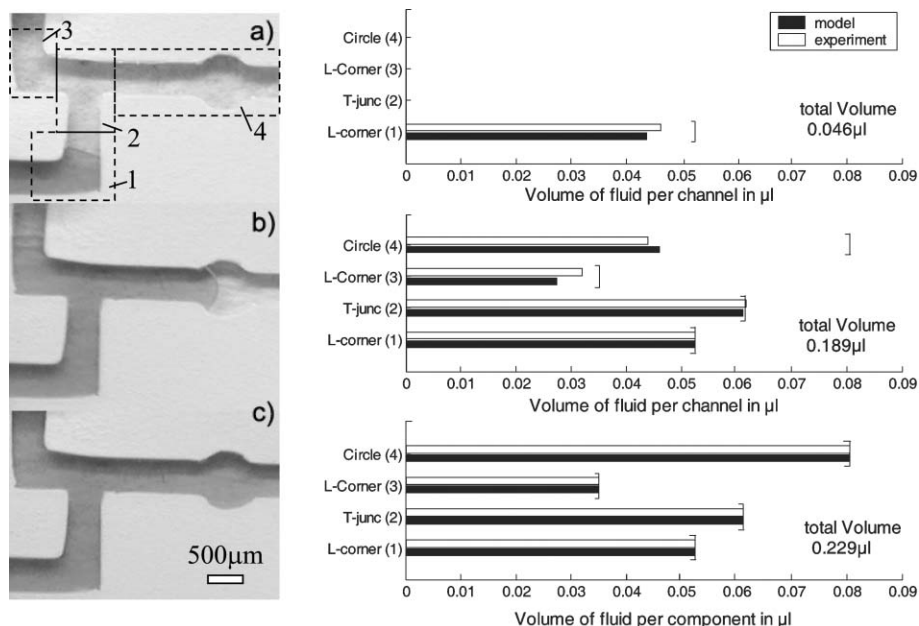
Fig. 11 Comparison of theory *versus* experiment for a network with four components. The experimental measured interfaces are shown on the left for three total liquid volumes (increasing from top to bottom). The liquid reservoir is at the bottom left and the dark grey shaded area is due to the 0.2% content by volume of red food coloring. The plot on the right shows the amount of liquid in each component measured experimentally (open bars) and predicted theoretically using the two part model of Section 3.6 (shaded bars). Each bar shows how much volume has been filled for the 1, 2, 3, or 4 "component" delineated by dashed lines on the left of the figure. The "]" symbols show the total available volume in each of the four components. The energy of the model and the experiment match to within 12%, 13%, and 4% respectively for the three cases shown.

design complex networks 'by hand'. This paper presents an effective, minimum-energy based model for simulation of fluid filling in passive, planar, micro-fluidic networks. The model follows a two-step process: the first step allows the simulation of components in minutes, the second step characterizes each component by an 'energy *versus* volume' curve and permits the simulation of networks with thousands of components in seconds. However, the model does not have a fluid dynamic component and it does not predict how fast the network will fill. Model results show accurate agreement with experiments for a variety of single component and small network shapes. Hence this paper presents a predictive, numerically efficient, modeling tool that will aid in the design of future lab-on-a-chip systems.

I. Treise, N. Fortner, B. Shapiro* and A. Hightower
Aerospace Engineering/Bio-Engineering, 3178 Martin Hall, University of Maryland, College Park, Maryland, MD 20742, USA. E-mail: benshap@eng.umd.edu

References

1 L. Y. Yu, Experimental investigation and numerical simulation of injection molding with micro-features, *Polym. Eng. Sci.*, 2002, **42**, 5, 871–888.

2 A. Daridon, Multi-layer microfluidic glass chips for microanalytical applications, *Fresenius' J. Anal. Chem.*, 2001, **371**, 2, 261–269.

3 M. A. Gretillat, A new fabrication method for borosilicate glass capillary tubes with lateral inlets and outlets, *Sens. Actuators, A*, 1997, **60**, 1–3, 219–222.

4 A. Manz, Electroosmotic Pumping and Electrophoretic Separations for Miniaturized Chemical-Analysis Systems, *J. Micromech. Microeng.*, 1994, **4**, 4, 257–265.

5 P. M. Martin, Laminated plastic microfluidic components for biological and chemical systems, *J. Vac. Sci. Technol., A*, 1999, **17**, 4, 2264–2269.

6 L. Martynova, Fabrication of plastic microfluid channels by imprinting methods, *Anal. Chem.*, 1997, **69**, 23, 4783–4789.

7 Z. Y. Wu, Polymer microchips bonded by O-2-plasma activation, *Electrophoresis*, 2002, **23**, 5, 782–790.

8 H. Becker and C. Gartner, Polymer microfabrication methods for microfluidic analytical applications, *Electrophoresis*, 2000, **21**, 1, 12–26.

9 O. Hofmann, P. Niedermann and A. Manz, Modular approach to fabrication of three-dimensional microchannel systems in PDMS—application to sheath flow microchips, *Lab Chip*, 2001, **1**, 2, 108–114.

10 Y. Feng, Passive valves based on hydrophobic microfluidics, *Sens. Actuators, A*, 2003, **A108**, 1–3, 138–43.

11 A. J. Przekwas H. Q. Yang and M. M. Athavale, Computational design of membrane pumps with active/passive valves for micro-fluidic MEMS in *Proc. SPIE—Int. Soc. Opt. Eng.*, 1999.

12 A. Puntambekar, A new fixed-volume metering microdispenser module based on sPROMs technology, in *Eurosensors XV, 11th International Conference on Solid-State Sensors and Actuators, Transducers*, 2001, Berlin, Germany, Springer-Verlag.

13 Y. C. Su and L. Lin, A Water-Powered Micro Drug Delivery System, *IEEE/ASME J. Microelectromech. Syst.*, 2004, **13**, 75–82.

14 C. H. Ahn, Disposable smart lab on a chip for point-of-care clinical diagnostics, *Proc. IEEE*, 2004, **92**, 1, 154–73.

15 N. Fortner, B. Shapiro and A. Hightower, Modeling and Passive Control of Channel Filling for Micro Fluidic Networks with Thousands of Channels, in *33rd AIAA Fluid Dynamics Conference and Exhibit*, Orlando, FL, American Institute of Aeronautics & Astronautics (AIAA), 2003.

16 P. W. Tuinenga, *SPICE : a guide to circuit simulation and analysis using PSpice*, 3rd edn., Prentice HallEnglewood Cliffs, N.J., 1995.

17 N. Fortner and B. Shapiro, Equilibrium and Dynamic Behavior of Micro Flows Under Electrically Induced Surface Tension Actuation Forces in *The 2003 International Conference on MEMS, NANO, and Smart Systems (ICMEMS)*, 2003, Banff, Alberta, Canada.

18 B. Shapiro, Equilibrium Behavior of Sessile Drops under Surface Tension, Applied External Fields, and Material Variations, *J. Appl. Phys.*, 2003, **93**, 9.

19 Y. Lin, Microfluidic Devices on Polymer Substrates for Bioanalytical Applications, in *IMRET3, 3rd International Conference On Microreaction Technology*, 1999, Frankfurt, Germany.

20 K. Brakke, The Surface Evolver, *Experimental Mathematics*, 1992, **1**, 2, 141–165.

21 J. M. Floryan and H. Rasmussen, Numerical methods for viscous flows with moving boundaries, *Appl. Mech. Rev.*, 1989, **42**, 12.

22 J. M. Hyman, Numerical methods for tracking interfaces, *Physica*, 1984, **12**, D, 396–407.

23 J. J. Monaghan, Particle methods for hydrodynamics, *Comput. Phys. Rep.*, 1985, **3**, 71–124.

24 S. Osher and R. Fedkiw, *Level Set Methods and Dynamic Implicit Surfaces*, Springer-Verlag, New York, 2003.

25 S. A. Sethian, *Level Set Methods & Fast Marching Methods*, 2nd edn., Cambridge University Press, 1999.

26 C. W. Hirt and B. D. Nichols, Volume of fluid (VOF) method for the dynamics of free boundaries, *J. Comput. Phys.*, 1981, **39**, 201–225.

27 R. P. Fedkiw, A non-oscillatory eulerian approach to interfaces in multi-material flows (the ghost fluid method), *Comput. Phys.*, 1999, **152**, 457–492.

28 R. Caiden, R. Fedkiw and C. Anderson, A Numerical Method for Two Phase Flow Consisting of Separate Compressible and Incompressible Regions, *J. Comput. Phys.*, 2001, **166**, 1–27.

29 A. C. Antoulas, D. C. Sorensen and S. Gugercin, A survey of model reduction methods for large-scale systems, *Contemp. Math.*, 2001, **280**, 193–219.

30 N. K. Sinha, Reduced-order models for linear systems in *IEEE International Conference on Systems, Man and Cybernetics*, IEEE, New York, NY, 1992.

31 D. Hinrichsen and H. W. Philippsen, Model reduction using balanced realizations, *Automatisierungstechnik*, 1990, **38**, 11.

32 A. M. S. Dahshan,A. S. Fawzy and Y. A. E. Sawy, *Comparisons of several model reduction techniques.* , IEEE, New York, NY, 1985.

33 S. Shokoohi, *A survey of model reduction techniques for large-scale systems*, West Virginia University, Morgantown WV, USA, distributed by Western Periodicals Co., 1984.

34 N. K. Sinha and G. J. Lastman, Reduced order models for complex systems—a critical survey in *IETE Technical Review*, 1990.

35 Y. G. Kevrekidis, Order Reduction for Nonlinear Dynamic Models of Distributed Reacting Systems, *J. Process Control*, 2000, **10**, 177–184.

36 B. C. Moore, Principal component analysis in linear systems: controllability, observability, and model reduction, *IEEE Trans. Automatic Control*, 1981, **AC-26**, 17–32.

37 E. J. Grimme, *Krylov Projection Methods for Model Reduction*, PhD Thesis, ECE dept., University of Illinois at Urbana-Champaign, Urbana-Champaign, 1997.

38 T. Penzl, *Algorithms for model reduction of large dynamical systems*, 2000, Sonderforschungsbereich 393, Numerische Simulation auf massiv parallelen Rechern, TU Chemnitz 09107.

39 A. Bultheel and M. V. Barel, Pade techniques for model reduction in linear systems theory: a survey, *J. Comput. Appl. Math.*, 1986, **14**, 3.

40 K. Willcox and J. Peraire, Balanced Model Reduction *via* the Proper Orthogonal Decomposition in *AIAA Computational Fluid Dynamics Conference*, Anaheim, CA, 2001.

41 L. Sirovich, Turbulences and the dynamics of coherent structures, parts I & II, *Quart. Appl. Math.*, 1987, **45**, 561–571.

42 W. R. Graham, J. Peraire and K. Y. Tang, Optimal control of vortex shedding using low order models—Part I: Open-loop model development, *J. Num. Meth. Engr.*, 1999, **44**, 7, 945–972.

43 R. Qiao and N. R. Aluru, A compact model for electroosmotic flows in microfluidic devices, *J. Micromech. Microeng.*, 2002, **12**, 5, 625–35.

44 F. G. Tseng, I. D. Yang, K. H. Lin, K. T. Ma, M. C. Lu, Y. T. Tseng and C. C. Chieng, Fluid filling into micro-fabricated reservoirs, *Sens. Actuators, A*, 2002, **97**, 8, 131–138.

45 H. Q. Yang and A. J. Przekwas, Computational modeling of microfluid devices with free surface liquid handling, *International Conference on Modeling and Simulation of Microsystems, Semiconductors, Cambridge, MA, Sens. Actuators*, 1998.

46 D. S. Kim, K. C. Lee, T. H. Kwan and S. S. Lee, Micro-channel filling flow considering surface tension effect, *J. Micromech. Microeng.*, 2000, **12**, 236–246.

47 R. F. Probstein, *Physicochemical Hydrodynamics: An Introduction*, 2nd edn., New York, John Wiley and Sons, Inc., 1994.

48 P. C. Hiemenz and R. Rajagopalan, *Principles of Colloid and Surface Chemistry*, 3rd edn., Marcel Dekker, Inc, New York, Basel, Hong Kong, 1997.

49 R. A. Brown and L. E. Scriven, The shape and stability of rotating liquid drops, *Proc. R.. Soc. London, Ser. A*, 1980, **371**, 1746, 331–57.

50 J. Bico and D. Quere, Self-propelling slugs, *J. Fluid Mechanics*, 2002, **467**, 101–27.

51 E. B. V. Dussan, On the spreading of liquids on solid surfaces: static and dynamic contact lines, *Annu. Rev. Fluid Mechanics*, 1979, **11**, 371–400.

52 P. G. de Gennes, Wetting: statics and dynamics, *Rev. Mod. Phys.*, 1985, **57**, 3, 827–863.

53 R. P. Feynman, R. B. Leighton and M. Sands, *The Feynman Lectures on Physics*, Addison-Wesley Publishing Company, 1964.

54 J. L. Troutman, *Variational Calculus with Elementary Convexity*, New York, NY, Springer-Verlag, 1983.

55 J. Nocedal and S. J. Wright, *Numerical Optimization*, Springer Series in Operations Research, Springer Verlag, 1999.